

The Critical Coupling Likelihood Method: A new approach for seamless integration of environmental and operating conditions of gravitational wave detectors into gravitational wave searches.

Cesar A. Costa ¹ and Cristina V. Torres ²

¹Louisiana State University
Department of Physics
202 Nicholson Hall, Tower Dr.
Baton Rouge, LA 70803-4001 USA

²LIGO Livingston Observatory
PO Box 940
Livingston, LA 70754 USA

E-mail: cesar.costa@ligo.org
cristina.torres@ligo.org

Abstract. Any search effort for gravitational waves (GW) using large scale interferometric detectors like LIGO needs to be able to identify if and when noise is coupling into the detector's output signal. The Critical Coupling Likelihood (CCL) method has been developed to characterize potential noise coupling and in the future aid GW search efforts. By testing two hypothesis about pairs of channels, CCL is able to identify undesirable coupled instrumental noise from potential GW candidates. Our preliminary results show that CCL can associate up to $\sim 80\%$ of observed artifacts with $SNR \geq 8$, to local noise sources, while reducing the duty cycle of the instrument by $\lesssim 15\%$. An approach like CCL will become increasingly important as GW research moves into the Advanced LIGO era, going from the first GW detection to GW astronomy.

PACS numbers: 04.80.Nn, 95.55.Ym, 07.60.Ly

1. Introduction

Detectable gravitational waves (GWs) are perturbations of the local space-time metric which are associated with distant astrophysical phenomena. According to general relativity, these perturbations travel at the speed of light and are generated by astronomical scale masses with time varying quadrupolar and higher moments. The main goal of the Laser Interferometric Gravitational-Wave Observatory (LIGO) is to detect GWs and use this information to study the astrophysics associated with these sources [1].

The LIGO detectors are now undergoing a major upgrade. This upgrade will increase the instrument's sensitivity, extending the binary neutron star (BNS) observational range from the current $\sim 20\text{Mpc}$ to 200Mpc [2]. This change in the observational volume should increase the expected observable rate of GW signals. Using the network of GW detectors, one can expect BNS detection rates to improve from $1/50\text{yr}^{-1}$ to 40yr^{-1} [3, 4]. In order to achieve such sensitivity, LIGO instruments will be completely refitted with advanced components and control systems. This new configuration is called Advanced LIGO (aLIGO). During the aLIGO operational era, the first GW detection will mark the beginning of gravitational wave astronomy.

As LIGO has matured, the searches for GWs have overcome many obstacles, such as minimizing computational costs of a search, working with limited human resources, and performing instrument characterization along with needed instrumental changes. Instrumental expertise and commissioning knowledge remain the most scarce resources for conducting GW searches. In all previous observing epochs, LIGO's search efforts have relied on some amount of post-facto study of potential signals and their characteristics. This process is usually referred to as follow-ups and has been a limiting factor on how quickly a search can be completed [5, 6].

The first GW detection will be thoroughly reviewed, using the resource intensive traditional followup style and detailed studies about the quality of the data containing the event will also occur. In an era of regular GW detection, human resource costly procedures such as the traditional follow-ups and post-facto data quality (DQ) studies should be minimized. The state of the instrument, and hence the DQ have a significant impact on the effectiveness of LIGO's GW searches. Current DQ efforts identify epochs of questionable data quality. The DQ is analyzed in subsets, starting with the best data available, and epochs of decreasing quality data are added to the analysis to increase the effective observing time of the GW detector [7, 8]. Upon completion or near the end of an analysis the results are either disregarded immediately or further scrutinized during the follow-up procedure to determine if the potential GW candidate is the signature of an actual GW signal [5, 6].

In this paper we are proposing a new method, the Critical Coupling Likelihood, to investigate instrumental behavior and DQ. This method is intended to quantify instrumental operating conditions. We will also remark on how this information could be integrated into future GW searches. The CCL method uses the same sources of information as current DQ investigation methods, though it is a significant departure from those methods [9]. LIGO's current DQ methods have been invaluable and used in some form for all previous science runs for studying instrumental behavior and noise coupling. These existing methods became the standard for investigating LIGO's DQ but in an aLIGO era they may no longer be optimal methods for DQ studies. Significant revisions to these methods or new methods may be needed in order to do DQ investigations in an aLIGO era [10].

Understanding preponderant non-Gaussian noise sources is compulsory so that one can isolate them during the search process without unnecessarily compromising the instrument duty cycle. These transient noise sources are typically the result of a local influence on the instrument. These transient noise sources can lead to false GW candidates. In order to uncover the sources of this coupled transient noise in LIGO data there are a large number of sensors, which are collectively referred to as instrumental and environmental monitors.

LIGO records information about the detector's operating environment and the control systems of the interferometer. This information is used to determine if a specific sampled time from the instrument's GW output signal is or is not an artifact produced by a noise transient in the system. In order to accomplish this, each of the sensors are analyzed individually to identify departures from their nominal behavior. The results of this analysis could be used to identify and discard noise transients occurring during times of questionable data quality as part of a GW search [8, 11]. We propose to improve GW searches by applying our method, the Critical Coupling Likelihood (CCL) Test. This test can integrate information about the instrument condition, and its environment directly into a search [5, 6].

2. The Critical Coupling Likelihood

CCL is a statistical method intended to quantitatively identify as many avenues of environmental-to-instrumental coupling as possible. To accomplish this, the CCL method is based on time coincidence between event pairs from preselected data streams. This pairing is done between the GW data stream (GW channel) and an auxiliary sensor data stream (sensor channel). This statistical method is intended to distinguish between real coincidences (coupling) and accidental coincidences, which are coincidences unlikely to be of physical interest.

It is reasonable to expect that any sensor will have some level of inherent noise. It is important that this noise be Gaussian in nature, and for well engineered equipment this is typically the case. CCL has been designed to be as insensitive as possible to the inherent Gaussian noise properties of a pair of sensors. This insensitivity to the unrelated Gaussian behavior between the data sets makes it possible to distinguish accidental coincidence from suspected coupling.

The paired GW and sensor channels are analyzed individually to identify interesting potential artifacts; the specific algorithm used is a matter of convenience. The artifacts used to perform this study were the results of post-processed data, that was analyzed using a time-frequency (TF) decomposition analysis. CCL uses at least two artifact properties, and for the purposes of this paper we chose to use the signal-to-noise ratio (SNR), and time of occurrence to create the CCL function. One could use other artifact properties like frequency, bandwidth, duration, etc and by using any combination of these measured one can construct CCL models which are variations of each other. All of these variants in principle can be used to identify suspected coupling.

Differentiating unrelated artifacts (accidental coincidences) from coupled elements relies on the creation of two models. The potentially interesting set of artifacts, the coupled model (foreground) P_f , describes the temporal relationship between the GW data output and activity in the instrument's environment. It also contains unrelated time coincidences (accidental coincidences), for this reason one needs a second set of artifacts. This second set, the uncoupled model (background) P_b , has no statistically

meaningful relationships between elements in the GW and sensor data streams. As the name implies CCL is a method capable of determining the likelihood of instrumental coupling being absent or present. In order to make this determination one would consider the ratio of the foreground model to a background model as follows

$$CCL \propto 2 \log_{10} \left(\frac{P_f}{P_b} \right). \quad (1)$$

In calculating this quantity one is evaluating the potential for coupling at a specific time, between the GW channel and an individual sensor channel paired to it. The two quantities P_f and P_b must be constructed from some information, the artifacts, sampled from the GW channel, and an associated sensor channel respectively.

For the GW channel, selection criteria are applied to restrict the number of identified artifacts (y_i) (i.e. frequency interval, SNR range, etc.), and this set is defined as

$$\mathbf{Y} = [y_1, y_2, \dots, y_m]. \quad (2)$$

For the sensor channel no restrictions are imposed all the artifacts (x_i) are used and this set is defined as

$$\mathbf{X} = [x_1, x_2, \dots, x_n]. \quad (3)$$

All data analyzed will need to be organized into sets derived from analyzing intervals of time where the GW data is uniform in behavior. The intervals of uniform behavior are dependent on detector configuration changes, the operating condition of the detector and changes in the underlying stationary behavior of the detector.

3. Sampling Method

Models from sufficiently sampled data sets \mathbf{X} and \mathbf{Y} will be needed to describe potential relationships between the instrument and environmental effects. The epoch of sampling validity is defined as a time interval when only trivial changes to the running state of the GW detector have occurred. In defining epochs this way, the unknown coupling function (system function) should be nearly stationary between the GW detector and environment [12]. The minimum amount of data required to build a reliable model is directly proportional to the rate of the sensor artifacts recorded and as such the total amount of aggregated time (samples) required to build each model will be sensor dependent.

There are two approaches for sampling the data that can be done for model construction. The first approach is to sample the GW data stream uniformly, requiring a minimum of number of samples per unit time, ϕ . The alternate approach favored for the CCL tests is to sample the GW data stream using combined conditions. First, a minimum overall sampling rate ϕ_{low} is imposed. This ensures that samples are taken over the entire model epoch. Then a second condition is imposed on the sample SNRs, ρ_0 which must be greater or equal to the first quartile for m artifacts, where m indexes all previously observed GW channel artifacts, regardless of SNR. For periods of high ρ a temporary increase on ϕ to a higher temporary sampling rate, ϕ' is used to preferentially sample periods where instrumental misbehavior is more likely. The sampling thresholds ϕ_{low} and ρ_0 , must be fixed for the entire sampling epoch used to construct the model. By using ϕ and ρ , it is possible to determine an instantaneous sampling rate which favors sampling times of instrumental malfunction. This hierarchical sampling approach is called targeted sampling.

4. Model Resolution

The statistical properties of the collected data sets can be expressed by a probability mass function (PMF)—the discrete form of a probability density function (PDF). Each model (coupled and uncoupled) is represented by a two dimensional (2D) conditional probability distribution (CPD) which associates SNRs in the GW channel and the sensor channel. The resolution of the CPD, is dependent on the observation epoch and the sensor channel paired with the GW channel. Due to the discrete nature of the data, the resolution of the CPDs and PMFs are finite.

The artifacts contained in data from either the GW or sensor, can be described by an unknown number of distributions. One can assume that real instruments should have a baseline noise component plus possibly one or more additional unknown distributions. The baseline noise should be Gaussian distributed, and after processing it with a TF decomposition algorithm, the associated artifacts will follow a Rayleigh distribution [13]. This distribution describes the largest component of the observed noise. Due to the large number of low SNR artifacts a minimum SNR threshold ρ_0 , is applied to keep the volume of recorded artifacts down, and anything that would be below this value is assumed to be part of the inherent instrumental noise. The following equation expresses the censored form of the Rayleigh distribution of SNRs as

$$R(x) = \begin{cases} \frac{x}{\sigma^2} e^{-\frac{x^2}{2\sigma^2}} & , x > \rho_0 \\ 0 & , x \leq \rho_0. \end{cases} \quad (4)$$

where σ is the shape parameter for the Rayleigh distributed SNRs of Gaussian noise where the shape parameter is typically of the order of one. The unavoidable censoring alters the way this distribution is normalized and will be discussed later in the paper.

In addition to the Gaussian noise component observed in LIGO data there is also an excess of outlier artifacts. It is reasonable to describe this excess as at least one additional distribution ‡. In reviewing a variety of data sets we empirically determined that the most reasonable way to describe the observed high SNR outliers is a modified Weibull distribution (MWD) [14]. The Weibull distribution used for our purposes varies slightly from the standard form for a MWD and it is described as follows:

$$W(z(x)|\alpha) = \begin{cases} \frac{k}{\lambda} \left(\frac{z(x) - \log \alpha}{\lambda} \right)^{k-1} e^{-\left(\frac{z(x) - \log \alpha}{\lambda} \right)^k} & , z(x) - \alpha > 0 \\ 0 & , z(x) - \alpha \leq 0 \end{cases} \quad (5)$$

where $z(x) = \log(x)$. The profile of such a distribution is determined by three parameters: the shape parameter k where $k > 0$; the scale parameter λ where $\lambda > 0$; the shift parameter α where $\alpha \geq 0$. The parameter α scales the overlap of distributions. A properly selected α parameter allows us to adjust the relative positions of the expected Rayleigh and Weibull distributions for an effective single probability distribution. Figure 1 shows how these distributions might look relative to each other. In some extreme cases, the dual distribution assumption will break down and other distributions can be added to cope with this breakdown. The method described in this paper is easily generalized to integrate additional $W_i(z(x)|\alpha_i)$

‡ This second distribution is observed in LIGO data. It can not be explained by Gaussian processes. It is mostly due to instrumental malfunction and environmental causes.

distributions to combat this occasional method breakdown, but this generalization can become computationally challenging [15].

We defined this custom probability distribution function $C(x|\alpha)$, as

$$C(x|\alpha) = \psi_1 R(x) + \psi_2 W(z(x)|\alpha), \quad (6)$$

where ψ_i with $i = 1, 2$ are scaling parameters denoting the amount of relative Rayleigh and Weibull based artifacts. The ψ values are expected to behave in such a way to satisfy

$$\int_{\rho_0}^{x_{\max}} C(x|\alpha) = 1 \quad (7)$$

and the normalization of the censored $R(x)$ will be absorbed into the parameter ψ_1 .

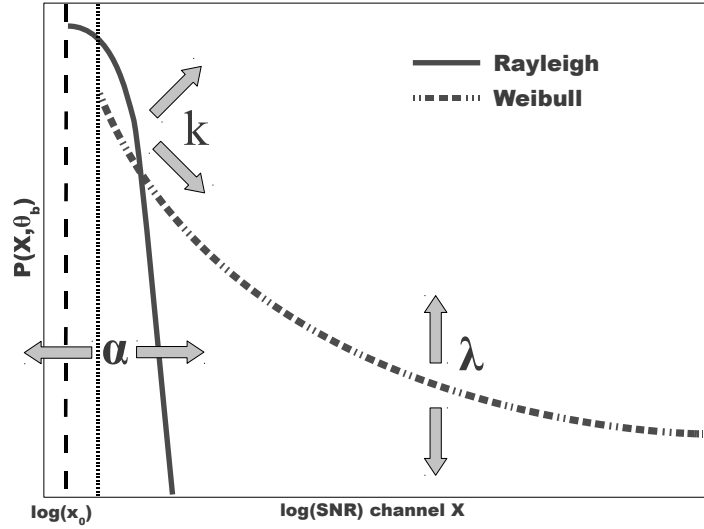


Figure 1: Background Model. We have determined empirically that background is composed of at least two distributions. The distributions shown start with a Rayleigh and is followed by a second distribution. The second distribution is assumed to be a Modified Weibull distribution. Together these model the distribution of CCL artifacts.

It is necessary to compute the discrete representation of $C(x|\alpha)$ in such a way as to best resolve all structure present. The histogram should have the most number of bins possible, without having an excessive number of near zero bin components. To construct such a histogram one needs to maximize the information entropy of the histogram [16]. The data sets contain a large range of observed SNRs, as such, it is better to discretize this data using logarithmically spaced bins rather than linearly spaced ones. Consider a set of bin edges which are base B logarithmically separated, the optimal choice of B can be determined by maximizing the total histogram entropy. Selecting B can be done iteratively, so that the resulting histogram of the data can easily be fit to the Rayleigh portion (low SNR) and also to the Weibull portion (high SNR) of $C(x|\alpha)$. To properly fit this function the entropy of the histogram as a function of B is computed. The value of B is expected to be somewhere in the interval $[2 \dots 10)$. One must also decide the number of bins b that should be used for histogram

construction. In order to determine the best binning to use one would simultaneously maximize the entropy of the histogram across both B and b . To discretely compute the entropy $H(x, b, B)$, requires computing the following quantity,

$$H(x, b, B) = -\sum_{i=1}^b v_i(x) \ln v_i(x) \Delta x_i \quad (8)$$

with the following normalization

$$\sum_{i=1}^b v_i(x) \Delta x_i = 1. \quad (9)$$

The width scale of Δx_i is logarithmically increasing by B , and the value of $v_i(x)$ is just the normalized element count in bin i . Optimizing the logarithmic scaling to the highest bin resolution possible is simply a matter of identifying the global maximum of $H(x, b, B)$. The most accurate fit to the data is possible when using a histogram representation with the highest reasonable entropy.

It is important that sampled data set properly represent the underlying distributions, in order to create a proper fit for $C(x|\alpha)$. Properly fitting the $C(x|\alpha)$ PDF involves determining the parameters, σ , α , λ , k , ψ_1, ψ_2 while respecting the threshold ρ_0 . The choice of which approach to determine the parameters is a direct consequence of the data set size, and ability to properly histogram the sampled data. Under typical circumstances, the approach of choice would be Quantile Maximum Product of Spacing (QMPS). In some cases the data sets are sparse. For this situation we use a fitting approach named Maximum Product of Spacing (MPS). The MPS approach uses all available data from the set and is inherently more tedious to apply than the QMPS approach. The two different approaches converge to the same parameters for data streams that are sufficiently sampled [17, 18].

The QMPS presented itself to be the most effective approach to determine the parameters of $C(x|\alpha)$. The cumulative distribution function (CDF) $c(\sigma, \alpha, k, \psi_1, \psi_2|x)$ of $C(x|\alpha)$ is defined from the CDF of $R(x)$

$$r(\sigma|x) = \begin{cases} \left(1 - e^{-\left(\frac{x^2}{2\sigma^2}\right)}\right) & , x > \rho_0 \\ 0 & , x \leq \rho_0 \end{cases} \quad (10)$$

and from the CDF of $W(x|\alpha)$

$$w(\alpha, \lambda, k|z(x)) = \begin{cases} 1 - e^{-\left(\frac{z(x) - \log \alpha}{\lambda}\right)^k} & , z(x) - \log \alpha > 0 \\ 0 & , z(x) - \log \alpha \leq 0. \end{cases} \quad (11)$$

These two equations can be combined into the following form

$$c(\sigma, \alpha, k, \lambda, \rho_0, \psi_1, \psi_2|x) = \psi_1 + \psi_2 - \psi_1 e^{-\left(\frac{x^2}{2\sigma^2}\right)} - \psi_2 e^{-\left(\frac{z(x) - \log \alpha}{\lambda}\right)^k}. \quad (12)$$

The parameters of interest are found by maximizing the quantity $S(\sigma, \lambda, k, \alpha, \psi_1, \psi_2|\mathbf{X})$

using QMPS as follows,

$$S(\sigma, \lambda, k, \alpha, \psi_1, \psi_2 | \mathbf{X}) = \prod_{i=0}^b \left(\psi_1 \left(-e^{\left(\frac{-\hat{x}_i^2}{2\sigma^2} \right)} + e^{\left(\frac{-\hat{x}_{i-1}^2}{2\sigma^2} \right)} \right) + \psi_2 \left(-e^{-\left(\frac{z(\hat{x}_i) - \log \alpha}{\lambda} \right)^k} + e^{-\left(\frac{z(\hat{x}_{i-1}) - \log \alpha}{\lambda} \right)^k} \right) \right)^{n_i}, \quad (13)$$

and all parameters can be fit simultaneously. Where n_i is the element count for the i th bin. The parameter \hat{x}_i represents the i th left side bin value which comes from the maximum entropy histogram of data which should represent the distribution $C(x|\alpha)$. Using this method will give us all the fitting parameters required to characterize the sampled data.

In the case that data samples are sparse, MPS is used to determine the parameters of interest. The MPS also seeks to maximize the quantity $S(\sigma, \lambda, k, \alpha, \psi_1, \psi_2 | \mathbf{X})$, but this approach varies as follows

$$S(\sigma, \lambda, k, \alpha, \psi_1, \psi_2 | \mathbf{X}) = \prod_{i=0}^j \left(\psi_1 \left(-e^{\left(\frac{-x_i^2}{2\sigma^2} \right)} + e^{\left(\frac{-x_{i-1}^2}{2\sigma^2} \right)} \right) + \psi_2 \left(-e^{-\left(\frac{x_i - \log \alpha}{\lambda} \right)^k} + e^{-\left(\frac{x_{i-1} - \log \alpha}{\lambda} \right)^k} \right) \right), \quad (14)$$

where j is the total number of elements x_i used to fit the parameters simultaneously. One should use QMPS whenever possible since implementing this calculation for very large j becomes computationally costly.

5. Creating Coupled and Uncoupled Models

Artifacts used to construct the coupled model are selected by applying a time coincidence check, with a window of t_w , which represents the largest absolute time difference between a GW channel artifact and sensor channel artifact. For this preliminary study we chose $t_w = 1$ s, after comparing a large collection of sensor data artifacts from many channels with GW data artifacts. When analyzing large sets of sensor channels, it is better to choose a t_w value which is long enough to capture all artifacts resulting from control loop delays, and physical delays between an environmental influence and the expected GW detector response to this influence.

The coupled model data P_f can be expressed as a conditional probability distribution (CPD) with the following form

$$P_f = P(\mathbf{Y} | \mathbf{X}, \theta_f) = \frac{P(\mathbf{Y} \cap \mathbf{X}, \theta_f)}{P(\mathbf{X}, \theta_f)} \quad (15)$$

where $P(\mathbf{Y} \cap \mathbf{X}, \theta_f)$ is a two dimensional joint probability distribution (JPD). This JPD represents the probability of a element in the set Y (GW data), given set X

(sensor data) for a specific model configuration θ . In this expression θ_f (foreground) denotes the set of samples drawn during potential coupling times.

The data used to construct the uncoupled model is derived from all available \mathbf{X} and \mathbf{Y} artifacts. Unlike the coupled model, the uncoupled model is intentionally designed to break the statistical relationship between the elements of \mathbf{X} and \mathbf{Y} . Using the PDFs of \mathbf{X} and \mathbf{Y} a background model JPD is built where we have forced statistical independence. This implies that the correct form for an uncoupled model's JPD, P_b is simply

$$P_b = P(\mathbf{Y} \cap \mathbf{X}, \theta_b) = P(\mathbf{X}, \theta_b) \cdot P(\mathbf{Y}, \theta_b). \quad (16)$$

To ensure the uncoupled model's discrete CPD matches the resolution of the coupled model's CPD, the discrete forms of $P(\mathbf{X}, \theta_b)$ and $P(\mathbf{Y}, \theta_b)$ must be consistent with their counterparts contained in $P(\mathbf{Y} \cap \mathbf{X}, \theta_f)$. In addition to knowing these functions one must also expect that the data which represents the coupling in the coupled model are not the dominate data source for constructing $P(\mathbf{X}, \theta_b)$ and $P(\mathbf{Y}, \theta_b)$. This additional constraint is easily satisfied when building models between any one particular channel and the GW channel. In a real world application of the CCL algorithm, there should be no one preferred source of coupled artifacts in the GW channel identifiable only by a single sensor input.

6. Calculation of CCL Function

The CCL function, introduced in equation 1, is the log likelihood ratio between the coupled and uncoupled models previously described, and should be expressed as follows:

$$CCL(\mathbf{Y}, \mathbf{X} | \theta_f, \theta_b) = 2 \log_{10} \left(\frac{P(\mathbf{Y} \cap \mathbf{X}, \theta_f) P(\mathbf{X}, \theta_b)}{P(\mathbf{Y} \cap \mathbf{X}, \theta_b) P(\mathbf{X}, \theta_f)} \right). \quad (17)$$

The above expression is easy to simplify algebraically because of equation (16) yielding

$$CCL(\mathbf{Y}, \mathbf{X} | \theta_f, \theta_b) = 2 \log_{10} \left(\frac{P(\mathbf{Y} \cap \mathbf{X}, \theta_f)}{P(\mathbf{Y}, \theta_b)} \frac{1}{P(\mathbf{X}, \theta_f)} \right). \quad (18)$$

The CCL function quantifies the level of suspected coupling between a specific sensor and the GW data. The observed CCL value can be translated into one of three statements: no coupling suspected; coupling suspected; or an indeterminate state with insufficient information to determine coupling. In the case of no coupling the CCL values will be negative indicating improbable coupling. For cases of coupling the CCL values will be positive indicating a potential GW channel candidate is likely due to a localized noise source influencing the GW detector. When the values are close to zero, either positive or negative, the test is incapable of determining whether the GW candidate is a noise artifact. There is no clear prescription for determining a single threshold on the CCL value that would be clearly indicative of coupling for all possible cases.

6.1. Visualizing and Interpreting CCL Function

Visualizing the CCL function offers insight into the characteristics of the data. One can consider these functions as a two dimensional color map with the GW data, $P(\mathbf{Y})$, plotted along the vertical axis and the sensor data, $P(\mathbf{X})$, plotted along the horizontal axis. When visualized preliminary functions we encountered distinct patterns in the

CCL values as a function of SNR between the two data sets. One might expect there to be some sort of pattern visible in the functions; found these patterns tend to be distinct. The distinctness of the patterns is attributable to the coupling mechanism described by the artifact distributions used to construct the CCL models (foreground and background). Upon reviewing many CCL plots, we noticed that they could be organized and characterized by specifically shaped regions in the CCL space occupied by high significance artifacts. Figure 2 presents an illustrative cartoon superimposing several key regions observed from different sensor data onto one graph.

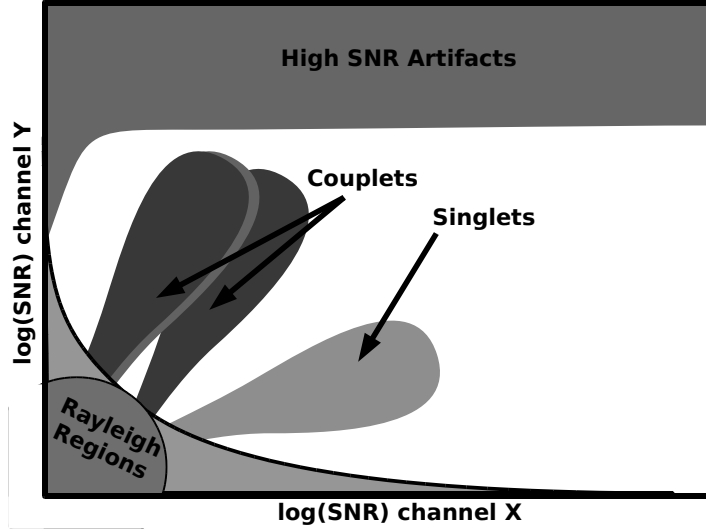


Figure 2: Coupling Regions: This figure contains several shaded regions. These regions illustrate typical structures but not all of which will manifest themselves in different CCL functions. The Rayleigh Noise, which is triangular in shape shown on the lower left is a region where differentiating a GW artifact from a noise artifact is not typically possible. The Singlets, and Couplets regions indicate potential coupling which is quasi-log-linear or quasi-bi-log-linear in nature. The High SNR Artifacts region is a boundary region where the linearity of the observed detector response for those artifacts is questionable.

The color map, represents the CCL values calculated for the data set. All CCL functions will contain some part of or all of a triangular region we call *Rayleigh Noise*, composed of three joined regions, one circular and two others triangular in shape (figure 2). The artifacts appearing in this region must be assumed to be related to Gaussian fluctuations in either the sensor or the GW channels. There is no way to distinguish Rayleigh artifacts, which are not coupled, from potentially coupled artifacts, which can lay in one of the two smaller triangular regions. Artifacts in these two smaller regions are the product of convolutions of inherent Rayleigh noise with potentially useful Weibull noise components. This convolution results in having only one of two pieces of useful information needed to identify coupling. For these two triangular regions CCL values here are typically near zero. This is different from the shaded circular region in figure 2 whose elements are composed from two pieces of

inherent noise which is Rayleigh distributed. For real data shown later, this shaded circular region can be less pronounced but is located in approximately the same region of the plot. In this case CCL values may take on a larger range of negative values. The three Rayleigh related regions are inherent to all CCL functions and are typically present in some form.

The next region of interest is the *Singlet* region. Here the CCL values show what appears to be a quasi-linear relationship in a log-log space of observed artifact's SNR in the sensor data compared with the artifacts in the GW data. Another region of interest is *Couplets* and this structure is normally seen in pairs of CCL functions. Consider two sensor channels that measure similar but not identical physical phenomena, like accelerometers and seismometers. Excessive ground motion at the detector might produce similarly distributed artifacts in both channels and CCL function plots will show overlapping parallel structures. The last region observed in most CCL functions, which is not sharply defined, is the *High SNR Artifacts* region. The events that compose this region are at the edge of linear behavior for differential arm motion sensing. Because of the potential for a non-linear instrument response, this region presents itself as unreliable [19]. These plots are useful as supplementary tools to visualize and help understand the relationships between the sensors and the detector output.

6.2. Disregarding CCL functions sensitive to gravitational waves

The detector should in principle have its output, the GW data, as the only data stream which is sensitive to GWs. In practice this is not guaranteed to be the case. The detector may have sensors which react to the presence of a GW. It is unwise and not safe to use a CCL function derived from sensors which may be responding to passing GWs. One needs a prescription for identifying sensor channels that are unsafe so those functions will not be used to identify non-GW artifacts in the detector output [8, 20].

An unsafe CCL function, with possible undesirable sensitivity to GW phenomena, can be identified with a simple prescription. If the CCL function is unsafe, then the distribution of hardware injections identified by an individual CCL function will be similar to the distribution of all artifacts due to hardware injections used to test the detector. Hardware injections are simulated GW signals introduced to the detector as a control signal that causes a physical response of the detector. It is the resulting response that is recorded in the GW channel [21]. Using these injections it should be straightforward to identify unsafe CCL functions. This identification process is accomplished by using a Kolmogorov-Smirnov (KS) test. The null hypothesis would be, "For a given sensor S , is the distribution of the hardware injection artifacts, identified with ($CCL \geq 1$) the same as the distribution of all known hardware injection artifacts?". A CCL function is tested for safety using

$$\sqrt{\frac{mn}{m+n}} \sup_x |F_{\theta_{f_{hw};m}}(x) - F_{all_{hw};n}(x)| \geq \kappa_\alpha, \quad (19)$$

with

$$F_a(x) = \frac{1}{a} \sum_{i=1}^a \begin{cases} 1 & \text{if } x_i < x \\ 0 & \text{if } x_i \geq x \end{cases}, \quad (20)$$

where x represents an SNR threshold, $F_{\theta_{f_{hw};m}}(x)$ represents the set of all hardware injection artifacts identified with $CCL \geq 1$ and $F_{all_{hw};n}(x)$ are all known hardware

injection artifacts. In applying our KS test, for a given significance level(κ_α) one would accept or reject the specified null hypothesis [22]. If the left hand side (LHS) of equation 19 exceeds the chosen κ_α then one should accept the null hypothesis because the hardware artifacts identified by the CCL function are being preferentially selected from set of all known hardware injections. Acceptance of the null hypothesis means that the sensor channel is unsafe. In the case that the LHS of equation 19 doesn't exceed κ_α , the sensor channel used to construct the CCL function is safe. This preliminary study required the boundary between safe and unsafe to be set by $\kappa_\alpha \leq 0.85$, which means that at the 85% confidence level we are sure of the safety or lack of safety for a tested sensor channel. This method of safety testing determined which sensor channels are safe and suitable for analysis with the CCL method.

7. Preliminary Results

We will show how the Critical Coupling Likelihood (CCL) method responds to artifacts in LIGO data, while ignoring effects that can be attributed to potential GW signals. The data used in this analysis is a set of sampled instrument times, which were pre-processed with a TF transformation tool called the omega pipeline. This tool was chosen primarily because this transformation used a wavelet decomposition basis which worked well for resolving signals with low frequency components [23]. The total aggregate time of our data samples is equivalent of 3.5 days of observing data, derived from sampling two months near the end of S6 for LIGO Livingston and LIGO Hanford observatories.

The costs of using CCL in the future are dependent on many factors. Using this case study we estimate an analysis rate which of approximately 10 to 20 times real time. The most costly phase of a CCL end to end analysis is the data pre-processing step. In order to apply CCL to an online detector one would need at least 1 compute core per every 5 to 10 sensor channels being analyzed. This estimate is reasonable if one assumes getting the sensor data to the compute core is instantaneous. The actual computational costs of the CCL method could be much higher depending on implementation of CCL, the pre-processor and data handling at each detector site.

The results presented here are intended to motivate the development of the CCL method, highlight typical CCL functions, and show encouraging results derived from a limited set of input sensors. The reader should bear in mind these results are a first attempt, a single case study using CCL, there remains a great deal of optimization, studies with larger sets and fine tuning to be performed.

The goal of a CCL analysis is to make quantitative statements about the instrument behavior relative to the studied sensor data. The CCL output is a single quantitative value, per available sensor data set, which is useful to determine the coupling state of the detector. The CCL functions have behaved differently when applied to LIGO Livingston in comparison with LIGO Hanford. This difference in behavior is unremarkable and attributable to the distinctly different operating environments.

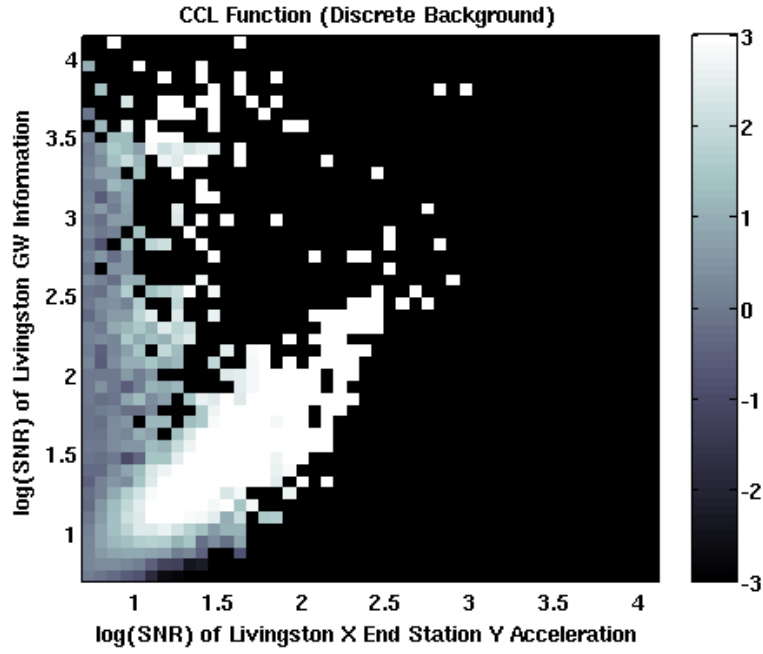
As an example, one of the many CCL functions generated, LIGO Livingston is plotted in figure 3a. The identifiable structure in this plot is an example of a *Singlet*. The singlet in this function is indicative of coupling to the instrument through seismic motion. The seismic motion induces an acceleration of an accelerometer mounted on an optics table in close proximity to one of LIGO's large optics(test mass). This optic is pitching back and forth while suspended at the end of one of LIGO's two arms

as a result of optical table motion. The optics increasing motion corresponds with increasing SNR of artifacts in the GW detector output. This relationship is readily seen in the figure as an angled structure of high CCL values.

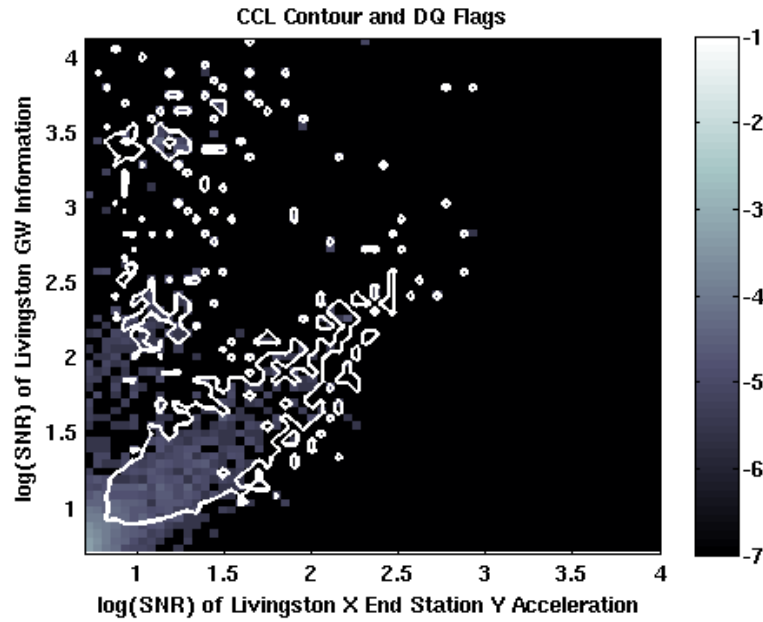
Examples of another type of CCL structure are shown using LIGO Hanford data in figures 4a and 5a. These figures show a different type of identifiable structure, a “Couplet”. For CCL functions with this type of structure, the artifacts identified by this model are typically in common with another sensor. In both figures, there appears to be two angled approximately parallel structures, not always easily distinguishable, but in this case one structure is better defined than the other. In figure 4a, the well defined angled structure corresponds to a poorly defined, but similar structure in figure 5a. This relationship is reciprocal, the well defined angled structure associated with figure 5a is the poorly defined structure associated with the couplet from figure 4a. The couplet structure appears in pairs of CCL functions. These pairs are usually related by obvious mechanisms as in demodulated signals or signals derived from mechanically interdependent systems. For these example figures, the two data channels are witnessing artifacts which are partially encoded as an in-phase and quadrature components of light received by the same photo-diode assembly. The in-phase component of light tracks common motion of the input optics which form the long Fabry-Perot arms of the interferometer. The quadrature phase tracks the differential motion of the input optic of the cavity. Laser power fluctuations can induce optic motion impacting the length of the Fabry-Perot cavities. These length changes can take the cavity off resonance and allow energy to exit the cavity. The energy exiting the cavity can transfer power from one arm to another leading to differential motion of the input optics. These two types of motion, common and differential, can excite one another and make controlling the full length interferometer difficult thereby increasing the noise in the interferometer.

The CCL method can provide a quantified measure describing coupling into the detector data. This measure is useful to understand if and what local environmental effects may be responsible for a false GW event. To appreciate the potential usefulness of a method like the CCL, we imposed a CCL threshold value. Thus exceeding this value declares an event as noise coupled to the detector. By using a CCL cutoff, $CCL \geq 1$, it allows us to sort the identified artifacts into two groups: inherent noise artifacts (uncoupled) and those which are due to environmental influences (coupled). This CCL value corresponds to an identified artifact is at least $\sqrt{10}$ times more likely to be coupled than uncoupled, as defined in section 6.

For LIGO Livingston, a total of 205 functions were used to identify the coupled artifacts. For LIGO Hanford, we used a total of 207 functions to identify the coupled artifacts in the Hanford data set. The set of artifacts analyzed were constructed by sampling Livingston and Hanford data with an average sampling rate of 1 sample, which is 1 second in duration, every two minutes using only science mode times. Science mode times are periods where the instrument is operating at the minimum level of data quality that should be considered viable to perform a search for GW signals [7]. Using this sampling constraint, the data set is less than 5% of the total amount of data available from two months near the end of LIGO’s sixth science run. We expect that if more samples were taken during the same interval of observation time the results of our preliminary analysis will remain relatively unchanged. Using these constraints on sampling rate and sensors used, figures 6 and 7 show the number of artifacts not identified as coupling after applying a CCL cut. For both figures, there is a clear suppression of the original outlier tails. What may not be readily



(a) CCL Function LLO (Singlet)



(b) CCL Function Contour includes DQ flags

Figure 3: In 3a we have an example of a “Singlet” structure, which shows a log-linear correlation between artifacts in the sensor and GW artifacts. In 3b the same information is shown as a shaded plot overlaid with contours denoting artifacts identified using current data quality analysis techniques[8]. One can notice that there is significant agreement between them. The noise in this example is related to increasing pitch motion of a large optic at the end of one detector arm. The accelerometer witnesses the increasing seismic motion because it is mounted on the assembly carrying the large optic.

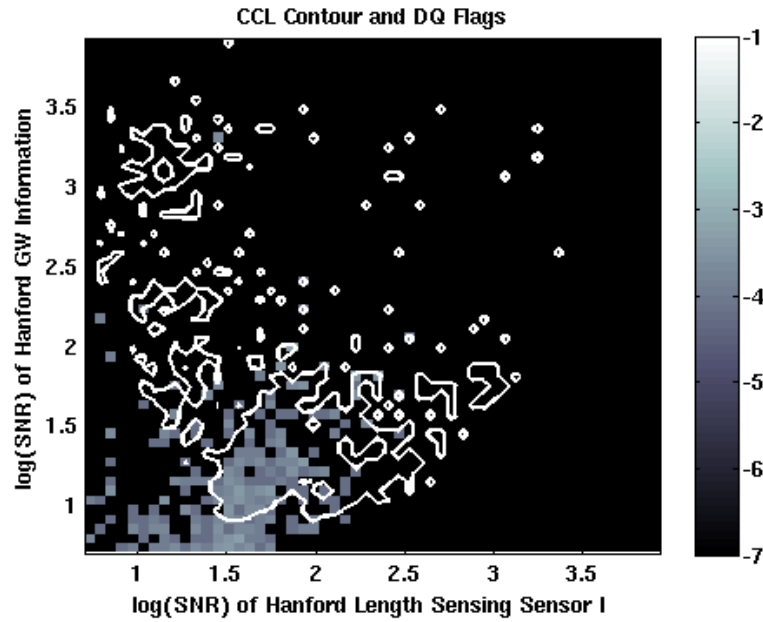
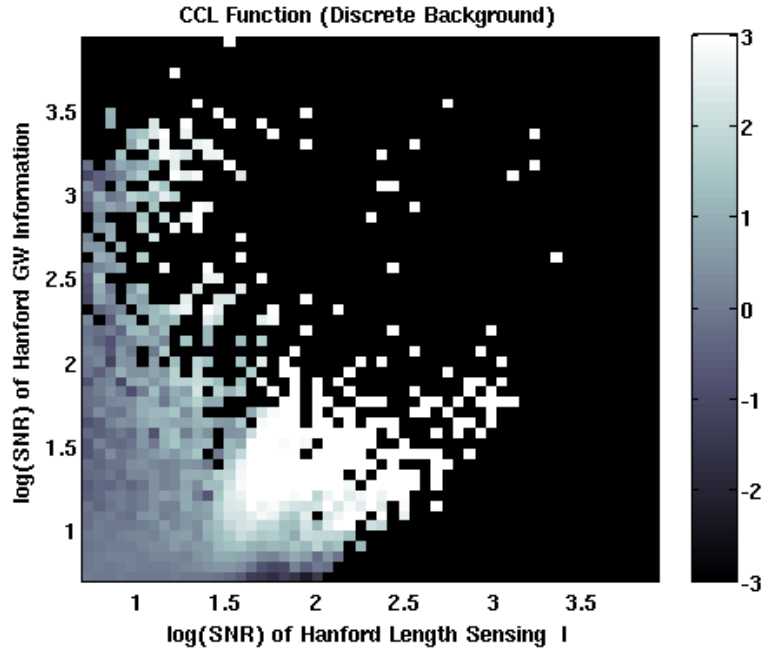
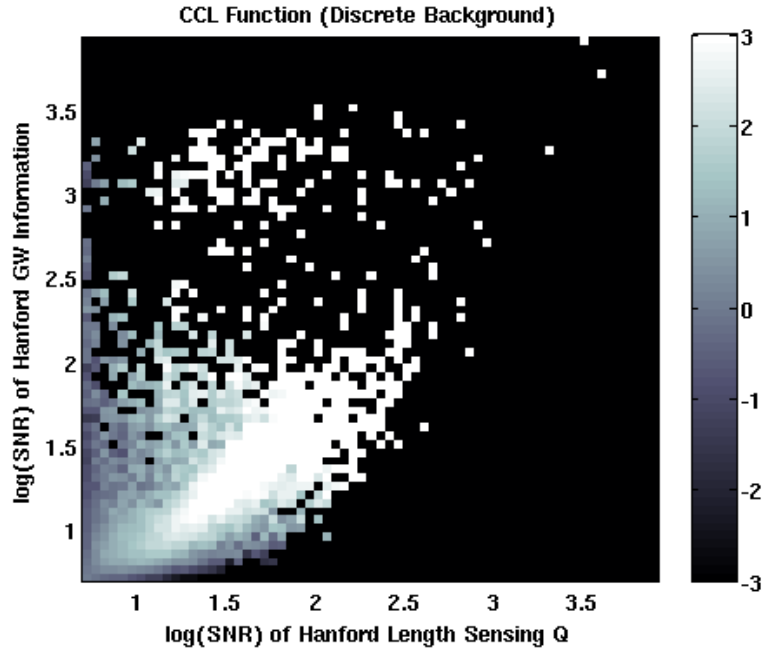
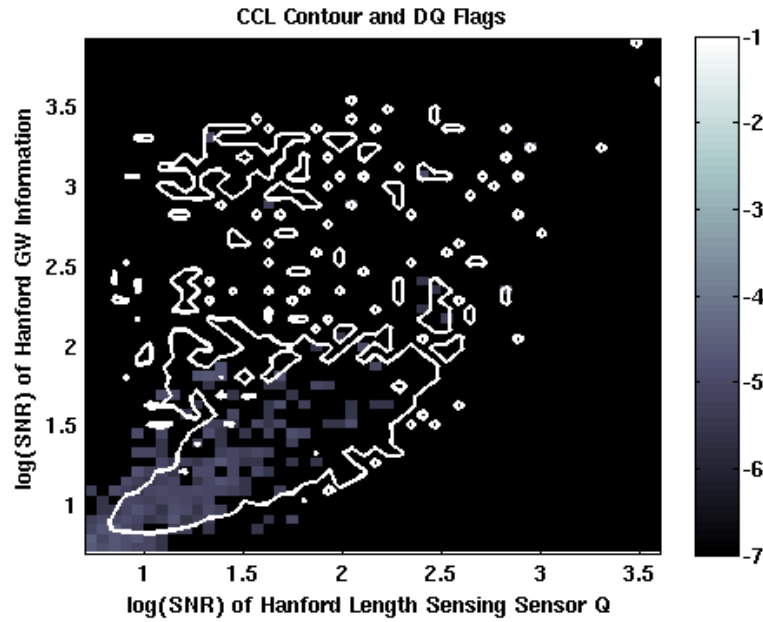


Figure 4: In 4a we have an example of a “Couplet” structure, which shows bi-modal correlation between artifacts in the sensor and GW artifacts. In 4b the same CCL information is shown as a shaded plot overlaid with contours denoting artifacts identified using current data quality analysis techniques[8]. In the contour plot the standard techniques show agreement for one half of the bi-modal region. The other half is identified in figure 5b. The noise shown is produced by excitations of common motion of the input optics making up the two Fabry-Perot arms of the interferometer.



(a) CCL Function (Couplet)



(b) CCL Function Contour includes DQ flags

Figure 5: In 5a we have “Couplet” structure shown in figure 4a. In 5b the CCL information is shown as a contour plot overlaid with artifacts identified using current data quality analysis techniques[8]. The contour plot shows agreement for one half of the bi-modal region. The other half is identified in figure 4b. The noise shown in this figure is produced by excitations of a differential motion between the input optics that form the Fabry-Perot arms of the interferometer.

	Livingston	Hanford
Deadtime	13.9%	15.1%
SNR(\geq)	%	%
5	14.4	16.3
8	82.3	93.5
10	88.8	96.7
20	86.7	98.0
50	92.4	98.9
100	98.0	99.2

Table 1: This is the efficiency and deadtime table for the Livingston and Hanford observatories. The deadtime estimated presented here is expected to be an upper limit on the expected deadtime for ($\mathbf{CCL} \geq 1$). Deadtime is analysis time which should be discarded because it is suspected of having to poor data quality characteristics [7].

apparent in these figures is that the CCL method appears able to suppress the outlier tail and identify moderate SNR artifacts, while leaving the original low SNR artifact distribution unchanged. In table 1, it is easier to see why one can appreciate the CCL method for identifying artifacts, because this method ignores SNR regions where artifacts tend to be the result of inherent noise properties of the instrument. This suppression of the outlier tail in this study is accompanied by a data volume cost. The amount of detector information that should be discarded, at least for this single case, is moderately high at 13.9% and 15.1% of the tested data for LIGO Livingston and LIGO Hanford respectively. A LIGO type detector has noise sources which are clearly non-Gaussian in nature. Some of these excesses have been identified, and are more pronounced in the LIGO's low frequency bands of (0Hz, 1kHz], which is thought to account for on order of 10%, of the excess outlier tail [9]. The artifacts contributing to the deadtime show a clear selection of non-Gaussian type artifacts. It is likely that our observed deadtime is not the result of our analysis configuration, but may actually be the product of an epoch which is less well behaved than one might expect. Further studies using CCL are called for but with this single case study there is already evidence that this method may prove to be beneficial for GW searches.

The sensor channels used in this preliminary study were those of the standard follow-up activities done at the end of a GW search [5, 6]. Using the safety prescription outlined in section 6.2 we discarded several channels suspected of presenting an undesirable sensitivity to GW phenomena and considered them potentially unsafe. According to such criteria, we were required to remove 10 channels for LIGO Hanford, and 9 channels for LIGO Livingston. Of the channels removed, a large fraction were consistent with channels suspected to be unsafe, with a few exceptions. One such unsafe channel noted for both detectors was the channels which records the amount of light incident on the detector's output mode cleaner. The light that is incident on the mode cleaner should contain the signature of a passing GW so, it would be unwise to use this channel as an indicator of detector noise. Not all, channels failing to meet the safety criteria were common to both detectors, in general the types of channels that were consistently seen as unsafe, were either related to the output of the detector or part of the feedback control of the detector.

One can see in table 2, that the remaining safe channels identify a small fraction of the total number of hardware injection artifacts. There is a notable contrast between

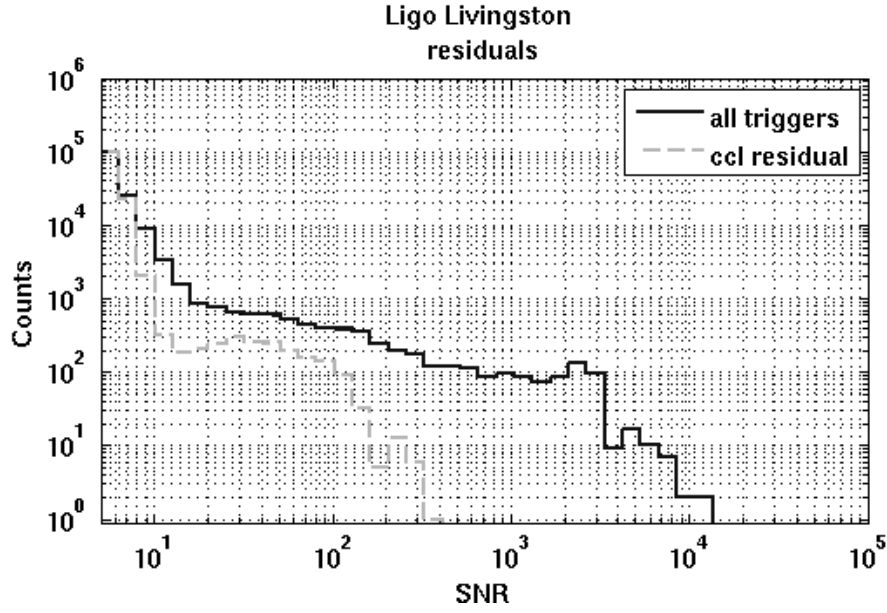


Figure 6: This figure shows the distribution of LIGO Livingston GW artifacts, as a solid curve. The dotted curve is set of remaining artifacts from the sampled set (solid curve) after removing ($CCL \geq 1$) identified artifacts.

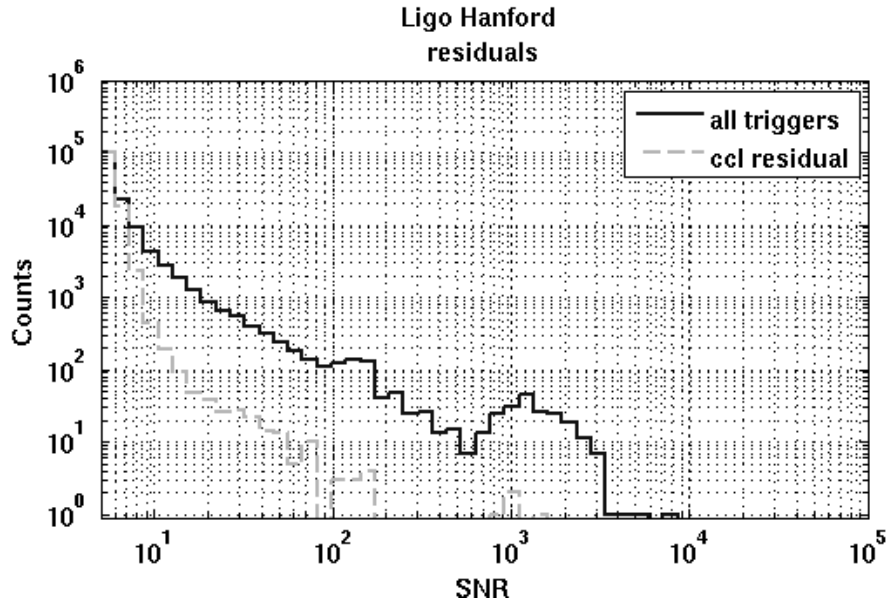


Figure 7: This figure shows the distribution of LIGO Hanford GW artifacts, as a solid curve. The dotted curve is set of remaining artifacts from the sampled set (solid curve) after removing ($CCL \geq 1$) identified artifacts.

Safe CCL Function Properties		
	Livingston	Hanford
Median Injection Count Per Channel	2	4
Mean Injection Count Per Channel	2.7(1.04%)	4.7(1.54%)
Standard Deviation on Count Per Channel	2.3(0.87%)	4.2(1.39%)
Hardware injection artifacts in data set	265	303
Total Number of Channels	205	207

Table 2: This table shows the average hardware injection artifacts identified per safe channel used in a CCL function. In these CCL functions the hardware injections identified are not consistent with all hardware injections performed, implying that these channels are safe for use to determine noise coupling in the detector.

Unsafe CCL Function Properties		
	Livingston	Hanford
Median Injection Count Per Channel	7	9
Mean Injection Count Per Channel	6.8(2.58%)	9.2(3.04%)
Standard Deviation on Count Per Channel	1.2(0.47%)	3.1(1.05%)
Hardware injection artifacts in data set	265	303
Total Number of Channels	9	10

Table 3: This table shows the average hardware injection artifacts identified per unsafe channel used in a CCL function. In these CCL functions the hardware injections identified are consistent with all hardware injections performed implying that these channels are unsafe for use to determine noise coupling in the detector.

the safe and unsafe functions, because as one can see from tables 2 and 3 the median number of hardware injections identified per CCL function for safe channels is much lower than those for unsafe channels.

8. Conclusions and Future Directions

The Critical Coupling Likelihood method is intended to improve future GW search efficiency and provide feedback to instrument scientists at the observatory. The results shown here are preliminary and are produced using a small set of LIGO data. The results shown use only the simplest form of CCL functions, capitalizing on the properties SNR and coincidence. We expect to see this same level of performance if we apply this approach to a full set of existing LIGO data or future aLIGO data. This method is promising because it offers quantified detector information which can be directly imported into a GW search. In creating this quantified detector information, the CCL method is also providing instrument scientists with information that describes potential coupling mechanisms between the instruments operating environment and behavior. We plan to present the instrumental implications of the CCL method in a later paper.

In this paper we introduced a new detector characterization technique called the CCL method. This method is intended to use all available observatory information and deduce the presence of coupling between the environment and the detector. In making this coupling identification it also implicitly estimates the coupling relationship

giving information about how the strength of local environmental effects map into specific noise levels and frequency bands. These preliminary results presented in this paper indicate that an approach like CCL should have an appreciable impact on the effectiveness of future GW searches, by reducing the outlier tail. Our initial results show CCL identifying $\sim 80\%$ of observed artifacts with $SNR \geq 8$. Identifying these outlier events lead to significant outlier tail suppression which is clearly seen in figures 6 and 7. By using this technique we can quantitatively characterize individual GW candidates, accounting for instrumental conditions, and hence improve GW searches and the validation of a detection.

9. Acknowledgments

The authors gratefully acknowledge the support of the United States National Science Foundation for the construction and operation of the LIGO Laboratory. The authors also thank LIGO and the LIGO Scientific Collaboration for allowing the use of LIGO data for this study. The authors would also like to acknowledge the support of this research via NSF grants PHY-0905184 and PHY-0757058. This paper was assigned LIGO document number LIGO-P1000187.

References

- [1] <http://www.ligo.org>
- [2] G. Harry et al., 2010 *Class. Quantum Grav.* **27** 084006
- [3] J. Abadie et al., 2010 *Class. Quantum Grav.* **27** 173001
- [4] I. Mandel et al., 2008 *ApJ* **681** 1431
- [5] C. V. Torres and R. Gouaty., 2010 *The Compact Binary Coalescence Search Follow-up the Home Stretch International School on Numerical Relativity and Gravitational Waves Asia Pacific Center for Theoretical Physics, Pohang Korea* LIGO-G1000679
- [6] R. Gouaty, 2008 *Class. Quantum Grav.* **25** 184006
- [7] B. Abbott et al., LIGO Scientific Collaboration, 2007 *Class. Quantum Grav.* **24** 5343
- [8] J. Slutsky et al., 2010 *Class. Quantum Grav.* **27** 165023
- [9] B. Abbott et al., 2009 *Phys. Rev. D*, **79**, 122001
- [10] LIGO Scientific Collaboration and Virgo Collaboration, 2011
<https://dcc.ligo.org/public/0062/T1100322/003/PublicWhitePaper.pdf>
- [11] B. Abbott et al., 2004 LIGO Scientific Collaboration *Phys Rev.D* **69** 122004
- [12] R. McDonough and A. Whalen, 1995 *Detection of Signals in Noise* **Academic Press**
- [13] N. Christensen et al., 2010 *Class. Quantum Grav.*, **27**, 194010
- [14] W. Nelson., 2003 *Applied Life Data Analysis* **Wiley-Interscience**
- [15] J. Hernandez and I. Phillips., 2006 *IEE Proc. Commun.* **153**, 2
- [16] R. Collins and A. Wragg., 1977 *J. Phys. A:Math. Gen.*, **Vol. 10** No. 9
- [17] R. Cheng and N. Amin., 1983 *J. R. Stat. Soc. Ser. B Stat. Methodol.* **45(3)** 394
- [18] D. Cousineau., 2009 *IEEE Trans. on Dielect. and Elect. Ins.* **16(1)** 281
- [19] J. Abadie et al., 2010 *NUCL INSTRUM METH A* **624** 223
- [20] N Leroy et al., 2009 *Class. Quantum Grav.* **26** 204007
- [21] D. Brown, 2004 *Class. Quantum Grav.* **21** S797-S800
- [22] Sheskin D., 2007 *Handbook of parametric and nonparametric statistical procedures* **4th ed** Chapman and Hall
- [23] Shourov K. Chatterji, 2005 *The search for gravitational-wave bursts in data from the second LIGO science run* **Ph.D. Thesis, MIT Dept. of Physics**